Peer-reviewed version available at Crystals 2018, 8, 440; doi:10.3390/cryst8120440

Optical Detection of Protrusive Defects on Thin-film Transistor

Fu-Ming Tzu[1] and Jung-Hua Chou[2]

[1]Department of Marine Engineering, National Kaohsiung University of Science and Technology, Kaohsiung, Taiwan, fuming88@nkust.edu.tw

[2]Department of Engineering Science, National Cheng Kung University, Tainan, Taiwan, jungchou@mail.ncku.edu.tw

[1]Correspondence: fuming88@nkust.edu.tw, Tel: +886-7-810-0888 ext. 25245

Abstract

Protrusive defects on the color filter of thin-film transistor (TFT) liquid crystal displays (LCDs) frequently damage the valuable photomask. An fast method using side-view illuminations associated with digital charge-couple devices (CCDs) to detect the protrusive defect in the four substrates, which are the black matrix (BM), red, green, and blue. Between the photomask and substrate, the depth of field (DOF) is normally 300 μm for the proximity-type aligner; we select the four substrates to evaluate the detectability in the task. The experiment is capable of detecting measurements of 300 μm and even lower than 100 μm can be assessed successfully. The maximum error of the measurement is within 6% among the four samples. Furthermore, the uncertainty analysis of three standard deviations is conducted. Thus, the method is cost-effective to prevent damage for valuable photomasks in the flat panel display industry.

Keywords: Protrusion, illumination, height, effective pixel, gray level, teaching

Peer-reviewed version available at Crystals 2018, 8, 440; doi:10.3390/cryst8120440

Introduction

The photomask is a cost component in patterning of optoelectronic devices [1-3]. With the booming market of liquid crystal display (LCD) TVs moving toward large panels, the geometric complexity of the photomask is increasing continuously. If the protrusive defect adhered onto the substrate goes through the photolithography process, the photomask will be damaged [4, 5] without warning. The photomask will bring about dramatic loss. Figure 1 illustrates mask scratches in the depth of field (DOF) at 300 μm between the substrate and photomask due to the presence of protrusions. Practically, the DOF depends on the requirement of the proximity-type aligner; normally the gap is from 100 μm and 350 μm in various products.

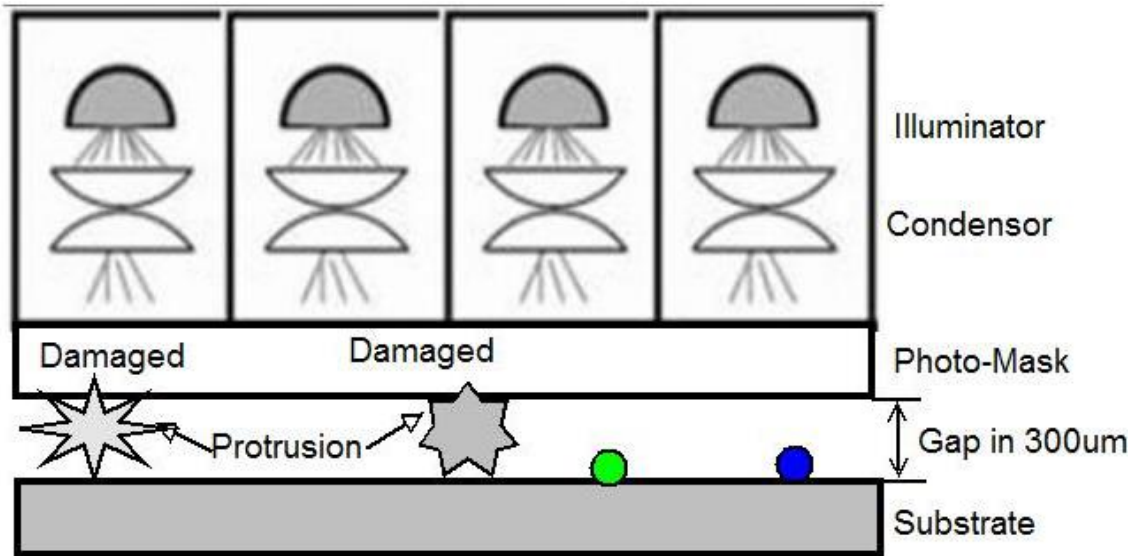

Figure 1 Photomask scratches due to protrusions.

Among protrusive defects, the statistics indicate the fragmented glass comprises 70%, the metal particles comprise 20%, and others make up 10% on the production line. Thus, the fragmented glass is the key factor in damaging the photomask. These efforts were made to delineate the related issues in the literature review in the past. For example, Ishii [6] utilized

a method for measuring the protrusion's 3D shape using a shape-from-focus scheme, in which the focused-section method reduced the contour of the shape. A ridge of 200 μm in height could be measured with a precision of 20 μm using an area charge-couple device (CCD). Ahmad and Choi [7] proposed a 3D window for finding the best focus points and applied it to a camera-mounted microscope for an auto-grinding equipment of LCD color filters. Zhang et al. [8] implemented and compared six known shapes from shading algorithms. The performance of the algorithms was evaluated by synthetic images using the mean and standard deviation of the depth error, the mean of the surface gradient error, and the central processor unit timing. In this study, we present a fast method to detect the protrusive defect that prevents photomask damage using a non-contact detection engaged in an CCD-based area. A cost-effective mechanism is installed on top of the platform through the side-view illumination method with an optical reflection in the dark field [9, 10] in the task.

Principle

The task utilizes the geometric reflectance optics to approach the albedo. The irradiance I is defined as the incident flux density (W/m^{-2}), whose expression is the following:[11]

$$I = \frac{d\phi_i}{dA} \quad (1)$$

The $d\Phi_i$ is the flux incident on the area (dA). The principle is based on the reflective shade to map an image with gray variation using CCD.[6, 8] After acquiring the image, the embedded algorithm computes the gray intensity for each pixel. Each gray level takes the baseline as the threshold. If the gray level is larger than the threshold, the level will count into the effective pixel. The average gray level of the effective pixels converts a relative

Preprints (www.preprints.org) | NOT PEER-REVIEWED | Posted: 24 September 2018 doi:10.20944/preprints201809.0463.v1

Peer-reviewed version available at Crystals 2018, 8, 440; doi:10.3390/cryst8120440

length in the range of 0~300μm of the protrusion that is with respect to 0~255 gray level. The average gray level lists in equation (2), in which the N_{pixel} denotes the effective pixels for which the gray level is greater than the threshold and the G_i labels a gray summation for effective pixel N_{pixel}.

$$Average_{gray} = \frac{\sum_{i=1}^{N_{pixel}} G_i}{N_{pixel}} \quad (2)$$

The $Average_{gray}$ represents the relative length of effective pixel while we perform the area conversation from square area to circular area. Figure 2 is an example representing each pixel of the gray intensity at the height 280μm of the protrusion on black matrix (BM) layer.

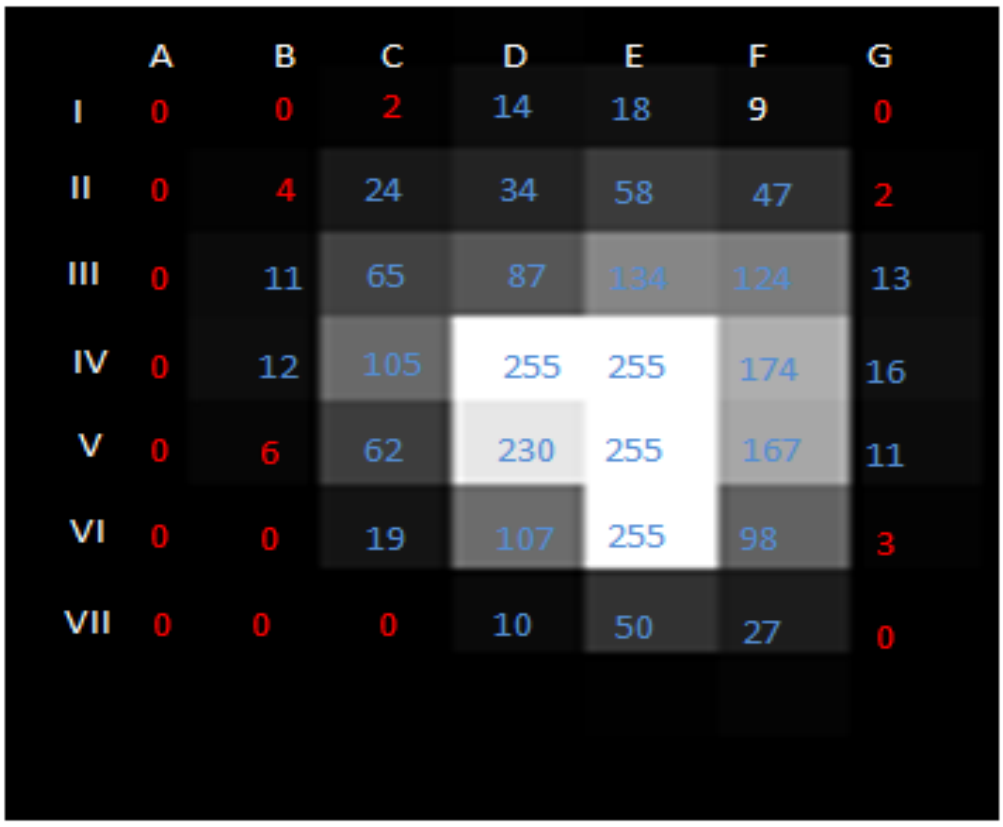

Figure 2 Protrusion displays the gray variety.

The pixel with blue-wise number labels the gray intensity which are the effective pixel.

Peer-reviewed version available at Crystals 2018, 8, 440; doi:10.3390/cryst8120440

On the other hand, the pixel with red-wise labeling are neglected, as their gray level is lower than the threshold intensity which are not effective pixels. Furthermore, equation (3) computes the round diameter (height) of the protrusion, in which *D* represents the equivalent diameter. The height of the protrusion is converted to the equivalent diameter from square area to circular area, the equation is as the following.

$$\sum_{1}^{N_{pixel}} L^2 * k = \frac{\pi}{4} D^2 \quad (3)$$

where the *D* is a diameter of the protrusion and *L* is length of effective pixel, *k* is a ratio parameter to teach a sample, and π is the ratio of the circumference. The image resolution depends on the optical working distances using the formula of a thin-lens maker. A rougher optical resolution indicates a large magnification field of view. With large generation LCDs driving the market, a non-contact area-scan is developed to investigate pseudo protrusive defects. In geometrical optics, the proper optical resolution design is shown in equation (4).

$$WD = \mathrm{f} * \left(\frac{M+1}{M}\right) + f * (M+1) + \overline{HH}^{*} \quad (4)$$

where *f* is the focal point; *M* is the magnification between the object and subject, $\overline{HH}^{*}$ represents the thickness of the lens, and *WD* is the optical working distance. While the scan is working, a signal capacitor array of a silicon epitaxial layer triggers the photo electronic current on the photoactive region. Each capacitor accumulates every electron charge so that it is proportional to the light intensity. Through the signal amplifier and decoding devices, the original signal is reconstructed by the shift register. Moreover, the task adopts the standard deviation to quantify the measured accuracy for the statistical population, which is the square root of the average mean from a set of data. The equation (5) is shown below:

Preprints (www.preprints.org) | NOT PEER-REVIEWED | Posted: 24 September 2018 doi:10.20944/preprints201809.0463.v1

Peer-reviewed version available at Crystals 2018, 8, 440; doi:10.3390/cryst8120440

$$\sigma = \sqrt{\frac{1}{n-1}\sum_{i=1}^{n}(p_i - \bar{p})^2} \quad (5)$$

where σ (sigma) is the symbol for standard deviation, $\bar{p}$ is the mean value from a finite dataset $\{p_1, p_2 \ldots p_n\}$, and $n-1$ is the finite population.

In the end, the task utilizes the side-view illumination to detect the protrusive defect then transforms its effective pixel to calculate its diameter.

Experimental Architecture

A schematic diagram using side-view illumination connecting an area CCD to detect the protrusion in the dark field is shown in Figure 3.

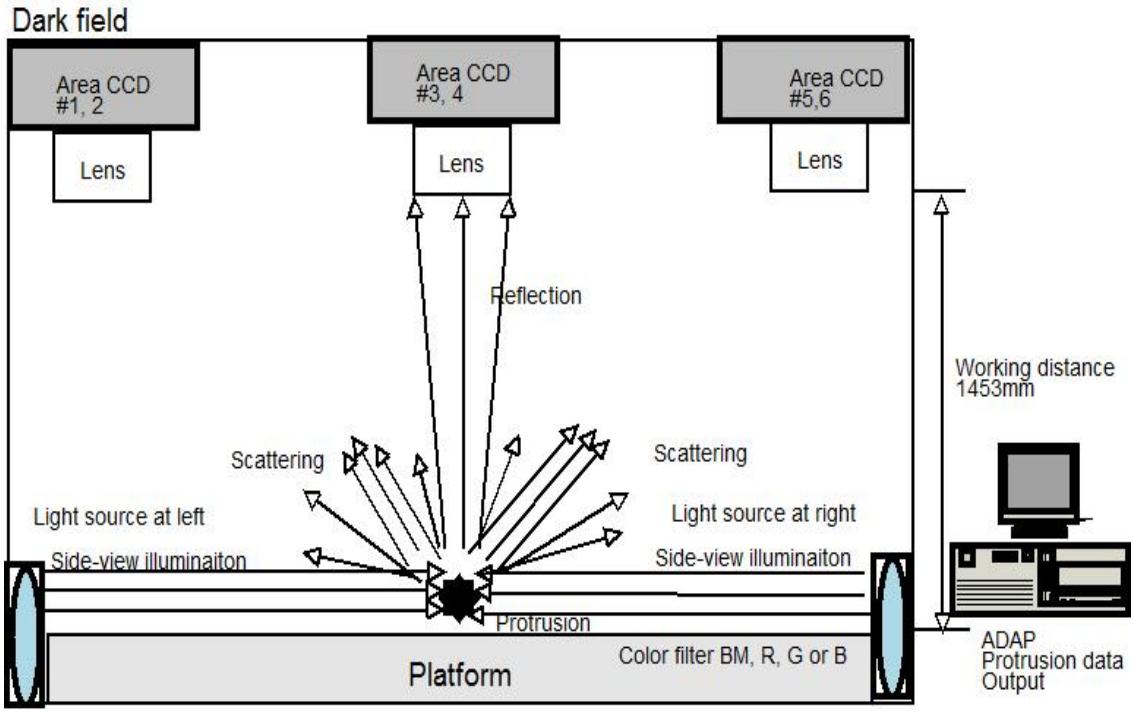

Figure 3 Schematic diagram associated with side-view illustration.

The protrusive detection system is installed on a flat platform on which two low-

pressure sodium lights connect the optical fibers to emit a set of parallel lights, in which the wavelength space is more than visual light. The platform of the tolerance in the horizontal is maintained at ±10 μm to ensure measurement accuracy. The experimental dimension accommodates the 6th generation TFT-LCD at size 1800 mm x 1500 mm. However, the optical system does not limit the detection area if the CCDs can extend to the whole field of view. The optical working distance is at 1453 mm from the substrate to lens (focal length 50-mm, f/2.8), whereas its optical path is calculated by equation (4). The parameter of the geometrical optics is tabulated in Table 1.

Table 1 Systemic specification for architecture detection

Items	Parameter	Descript	Length	Width
Optical resolution (μm)	200	Substrate dimension (mm)	1,800	1,500
CCD Pixel Size (μm)	7.4	Signal CCD FOV (mm)	650	974
Magnification	27	Require CCD quantity	3	2
Focused lens (mm)	50	Signal overlap (mm)	30	112
Working distance (mm)	1,453	All overlap (mm)	590	750
CCDs	6	Captured area (mm*mm)	1,770	1,500

The photo sensor is a regular 8-bit, 256-gray-scale, commercial off-the-shelf industrial area CCD with 30 frames per second. The pixel resolution is 4872*3248 pixels and the field of view is 650 mm*974 mm (length*width). An automatic data acquisition program is used to obtain the height of the specific protrusion. The innovative method has free-protrusion detection and the technique presents a fast, cost-effective, and reliable inspection after the production to 90% accuracy. Ordinarily, when the substrate loads to the platform in-line, the image is captured by the area CCD through the automatic data acquisition program. Then, the data output is performed automatically. Moreover, the spectrum of the light source is selected from 490 nm to 1050 nm so that the task filters out the ultraviolet spectra to avoid overexposure of the substrate. Experiments are conducted in a 100-class clean room.

Results and Discussion

Peer-reviewed version available at Crystals 2018, 8, 440; doi:10.3390/cryst8120440

The task employs the detected method engaging with the digital image process to intercept a specific protrusion. There are four kinds of samples to be dispatched at various fields of view, in which the glass balls are uniformly coated with film by the black matrix (BM), and red, green, and blue photo resists (PRs), respectively. The circle receives the light from the global directions, their reflectivity is even more than that of other shapes. The measurement uses coaxial light by the microscope, which is processed by Photoshop software. Their diameters are 280 μm, 277 μm, 256 μm, and 265 μm with respect to BM, red, green, and blue PRs, as shown in Figure 4.

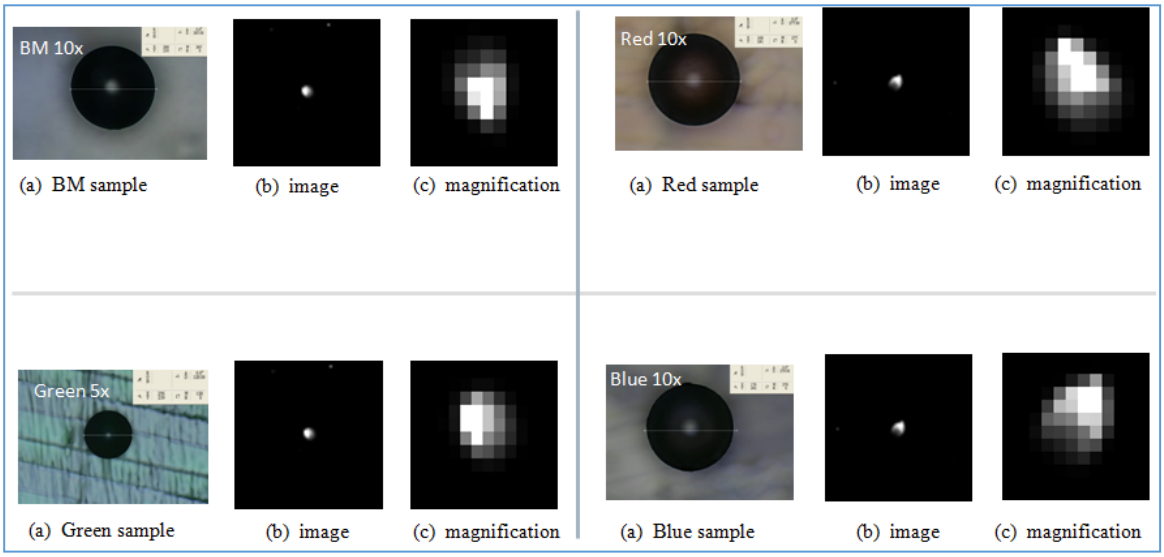

Figure 4 Various samples with different imaging for magnification.

Figure 5 illustrates the spectra of these BM, red, green, and blue thin-film coated balls (referred to as films for simplicity), which are detected by a spectrometer with an optical resolution of 0.8 nm (BTC611E, back-thinned CCD array, working wavelength from 300 nm to 1050 nm, produced by B&W TEK). The light sources are 250 W low-pressure sodium lamps since their brightness can illuminate the whole region to be detected to satisfy the threshold of gray level. The optical characteristics of the glass ball with BM film exhibit a

black body radiation response with low reflectivity compared to that of reference air. The largest response is 26% at 550 nm. The other visual wavelength for optical response is below 10%. By contrast, the PRs demonstrate higher reflections of the spectrum distribution, and the red film can shift energy between 600 nm and 750 nm. Thus, its reflective response is larger than the reference curve due to the red film characteristics.

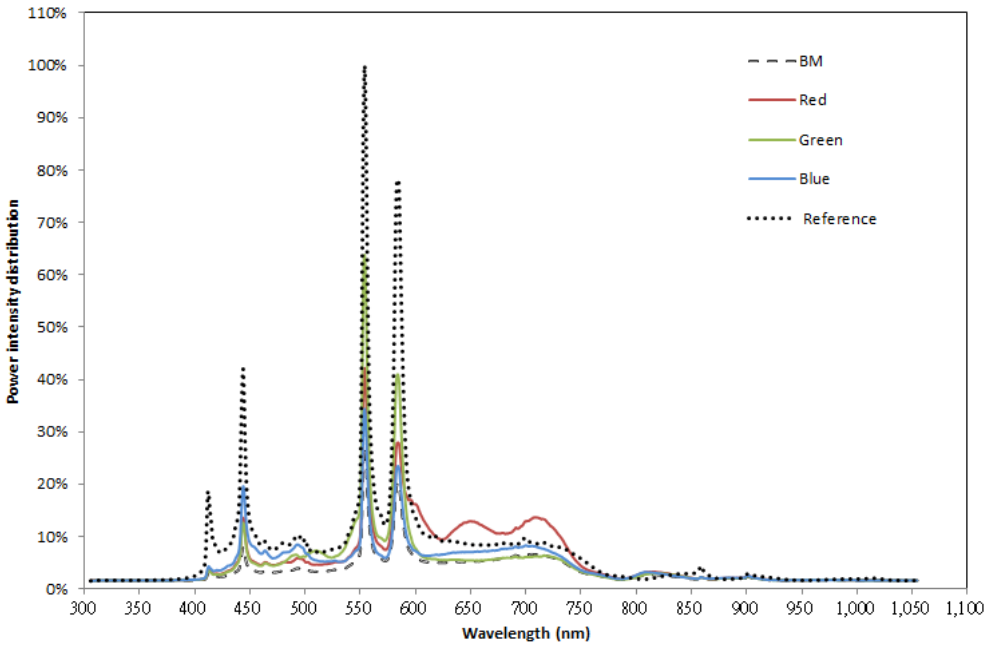

Figure 5 Spectrum distribution for various samples.

To obtain a reliable measurement, the threshold of the gray level depends on the reflectivity so that choosing the length of the effective pixel is induced the height of the protrusion. A teaching method also applies a set of *k* ratio that correct dark field at different samples before the measurement is performed. In Figure 6 indicates the *k* ratio is an exponential function proportional to the height of protrusion from 100 μm to 300 μm.

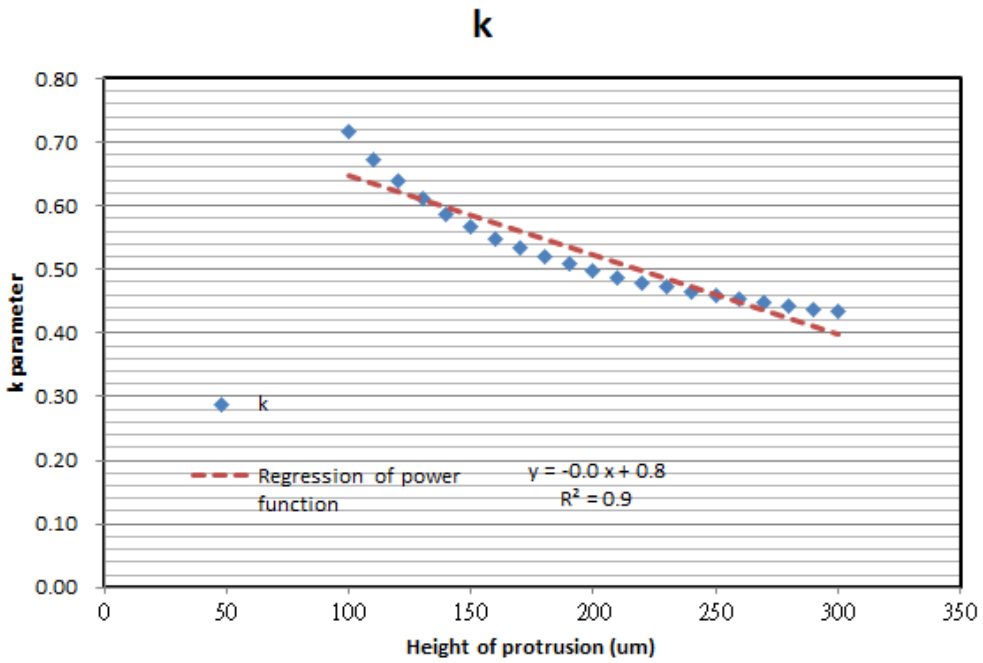

Figure 6 *k* parameter trends for teaching in the dark field

In this task, there are six CCDs to be installed on the ceiling that the area-scan covers all fields of view. Before the protrusive height measurement is implemented, the neutralization technique using a matrix 7*7 (row*column) template is a necessary teaching, such as CCD#5. Therefore, six CCDs cover the 21 rows (1~21 row horizontally) and 14 columns (I~IVX in symbols vertically) of the matrices as shown in Figure 7. Furthermore, Figure 8 indicates a stronger *k* ration in the middle space of optical field since BM is the almost black body that absorbs all incident light. Figure 9~11 is shown the less *k* ratio since the colored films reflects the light to stimulate the area-CCD so that its curve is different trend.

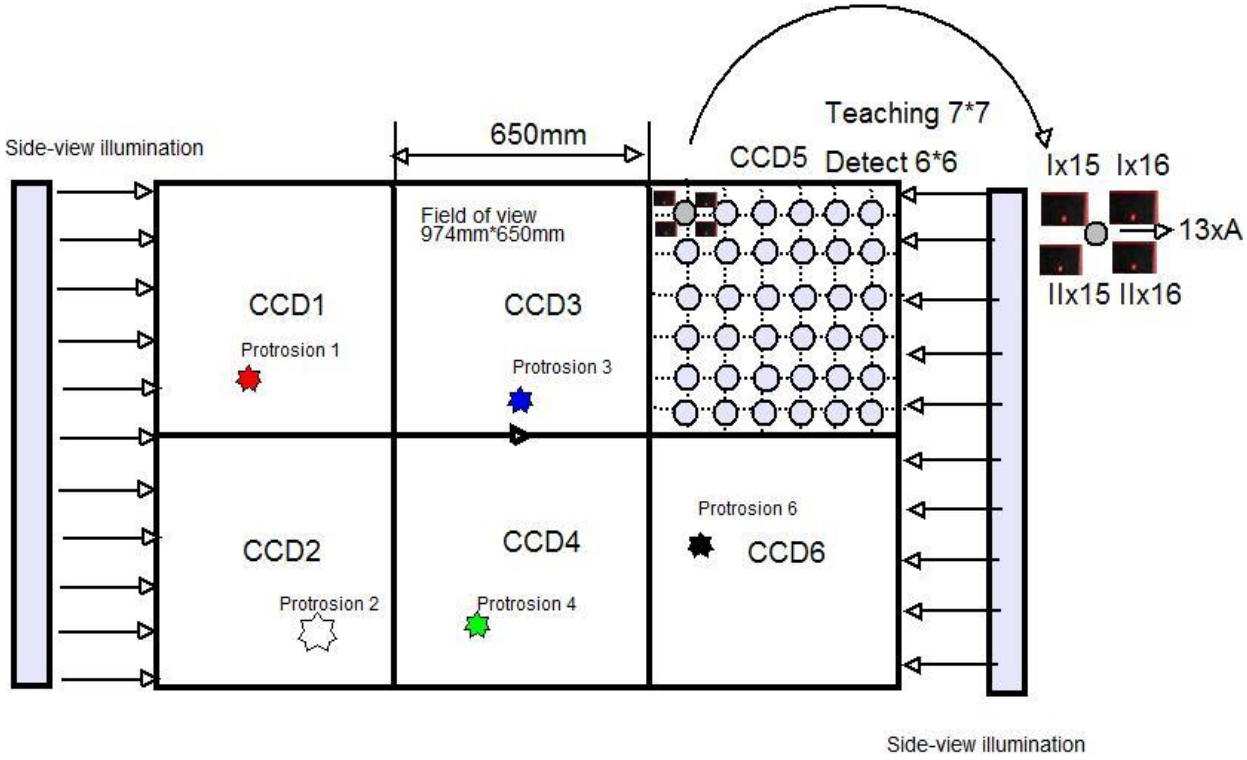

Figure 7 Topology of six CCDs in field of view for teaching template

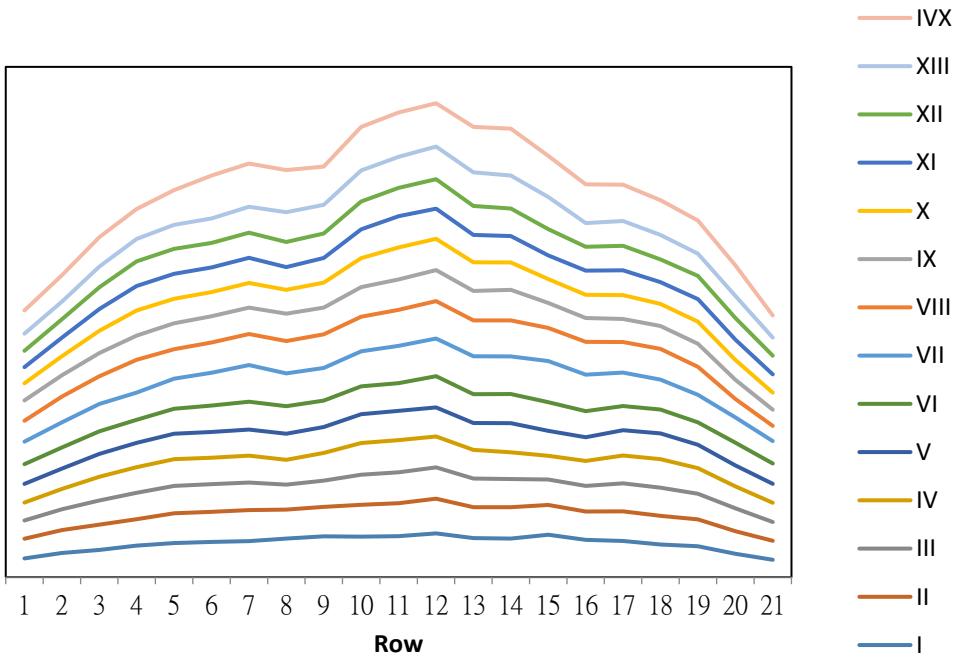

Figure 8 The tendency of the teaching in dark field for BM

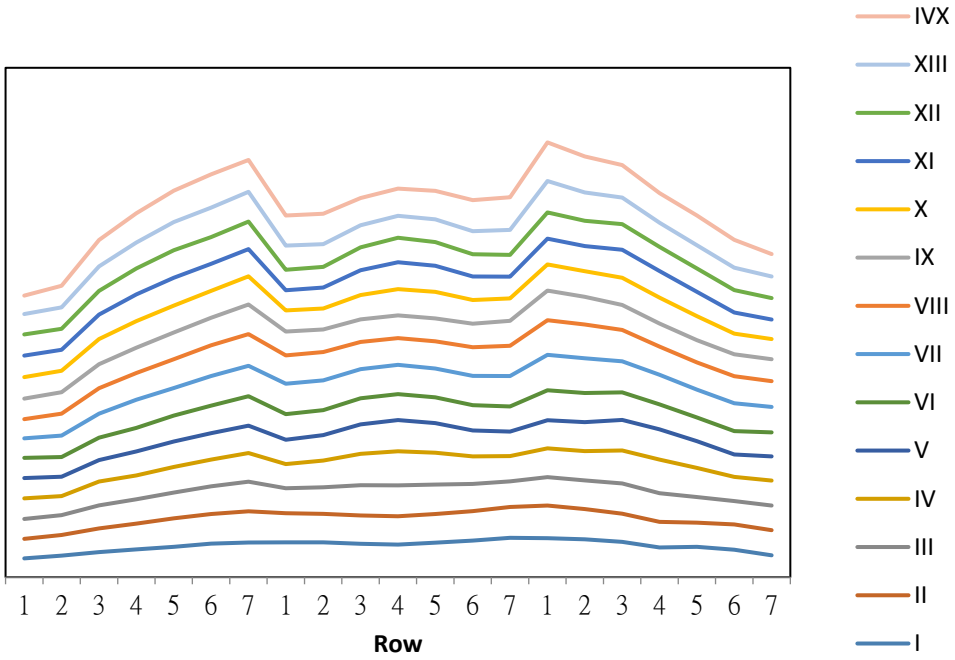

Figure 9 The tendency of the teaching in dark field for red

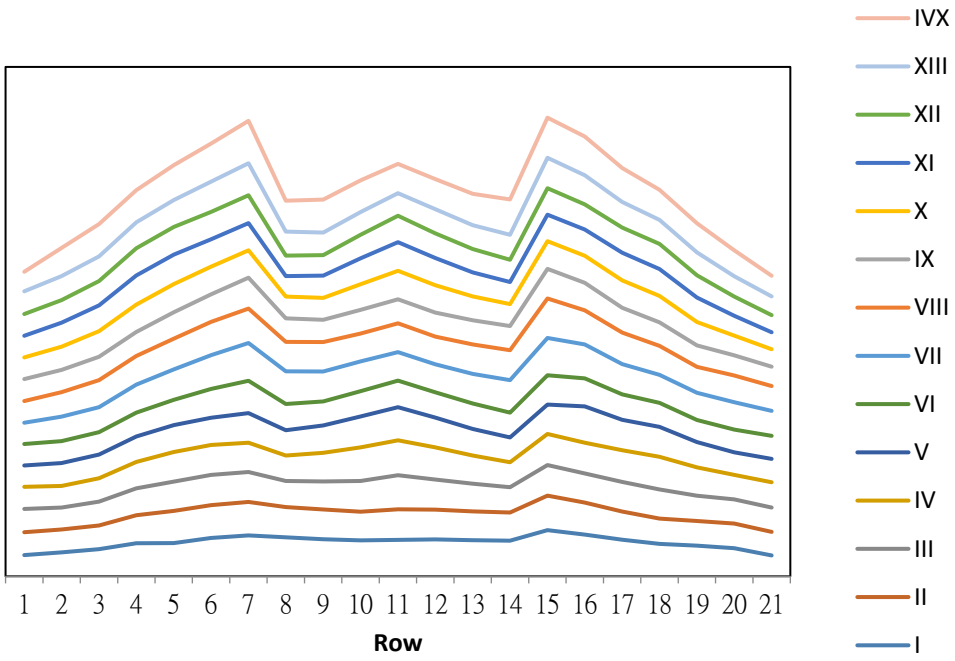

Figure 10 The tendency of the teaching in dark field for green

Preprints (www.preprints.org) | NOT PEER-REVIEWED | Posted: 24 September 2018 doi:10.20944/preprints201809.0463.v1

Peer-reviewed version available at Crystals 2018, 8, 440; doi:10.3390/cryst8120440

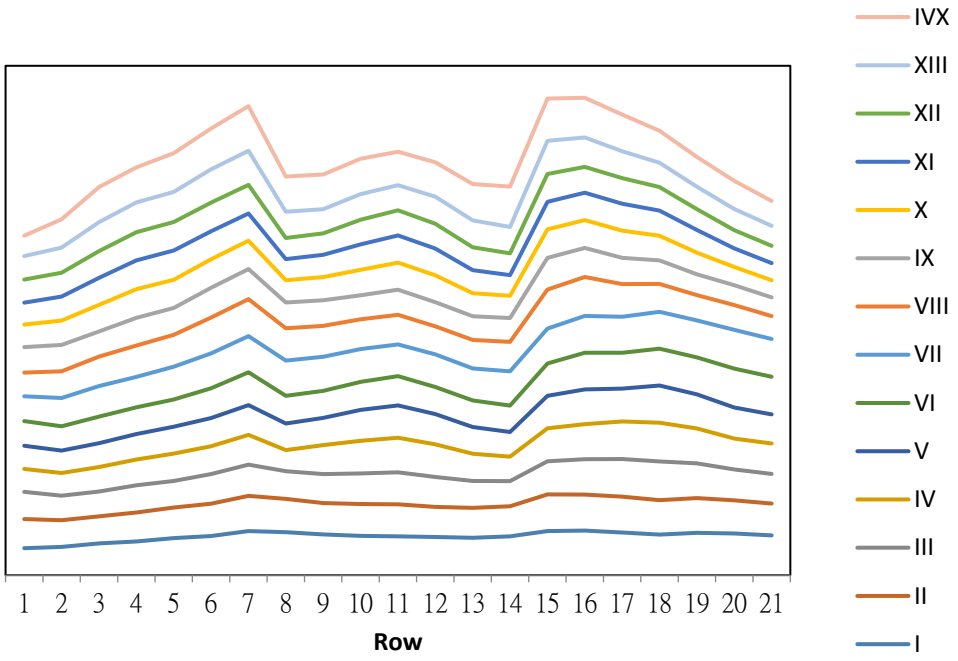

Figure 11 The tendency of the teaching in dark field for blue

These samples are placed on the test platform which are known its diameter as an analogy of the protrusive defects detected in this task. Table 2 shows a average height at 278 μm by means of 36 repeated measurements for the BM ball, which are at a maximum height at 299 μm and minimum height at 262 μm; an error shows the range from 6% to 7%. The uncertainty analysis is shown using three standard deviations at 25 μm.

Table 2 Results for detected protrusion on BM film

CCD#	Diameter(μm)	$Mean_{36times}$	Max(μm)	Min(μm)	Max_{error}(%)	Min_{error}(%)	3 σ(μm)
1	280	278	299	262	7%	6%	25
2	280	279	297	265	6%	5%	24
3	280	285	300	262	7%	6%	28
4	280	280	293	267	5%	5%	21
5	280	282	295	267	5%	5%	20
6	280	266	289	260	3%	7%	18
Average	280	278	296	264	6%	6%	23

Table 3 illuminates an average height at 275 µm with the means of 36 repeated measurements for the red ball, which compares the known height at 277 µm. However, its height variation is from 283µm to 266 µm, which is in the range from 2% to 4%. The three standard deviations show the variety at 13 µm at the 99.7% conference interval for uncertainty evaluation.

Table 3 Results for detected protrusion on red film

CCD#	Diameter(µm)	$Mean_{36times}$	Max(µm)	Min (µm)	Max_{error}(%)	Min_{error}(%)	3 σ(µm)
1	277	274	283	266	2%	4%	13
2	277	276	287	267	4%	4%	13
3	277	275	283	267	2%	4%	13
4	277	274	290	264	5%	5%	17
5	277	275	284	266	3%	4%	15
6	277	277	290	263	5%	5%	19
Average	277	275	286	266	3%	4%	15

Table 4 presents the tabulation of the detected protrusion at average 252 µm for a green ball, which is the same as the BM and red, taking 36 repeated measurements. Their height variation is in the range from 267 µm to 242 µm; an error measurement is 8% to 5%, from maximum to minimum.

Table 4 Results for detected protrusion on green film

CCD#	Diameter(µm)	$Mean_{36times}$	Max(µm)	Min (µm)	Max_{error}(%)	Min_{error}(%)	3 σ(µm)
1	256	253	276	242	8%	5%	22
2	256	252	266	240	4%	6%	15
3	256	251	265	241	4%	6%	18
4	256	254	265	245	4%	4%	17
5	256	253	269	241	5%	6%	22
6	256	253	263	241	3%	6%	16
Average	256	252	267	242	4%	6%	18

Table 5 shows the sample height at 265 μm that detects the protrusive height at average 262 μm for blue ball. Their height variation is in the range from 274 μm to 254 μm; an error measurement is 3% to 4%, from maximum to minimum, accordingly.

Table 5 Results for detected protrusion on blue film.

CCD#	Diameter(μm)	$Mean_{36times}$	Max(μm)	Min (μm)	Max_{error}(%)	Min_{error}(%)	3 σ(μm)
1	265	258	274	254	3%	4%	16
2	265	263	279	248	5%	6%	21
3	265	264	276	249	4%	6%	21
4	265	262	277	245	5%	8%	22
5	265	262	278	247	5%	7%	21
6	265	261	273	247	3%	7%	18
Average	265	262	276	248	4%	6%	20

As a result, the sample of the BM ball shows the lowest reflectivity to reflect the smallest irradiations among the PRs in order for the black color to absorb the most rays. The BM ball has the worst measurement in which the averaged three standard deviation measure is 23 μm compared to the red ball at 15 μm, the green ball at 18 μm, and the blue ball at 20 μm. On the other hand, the maximum and minimum errors are shown at 6% in contrast to the red, green, and blue balls at 3%~4%, 4%~6%, and 4%~6%. Thus, the colored balls illuminate better measurements than the black ball since these color-film balls irradiate stronger gray intensity.

Conclusions

An innovative technique employing a symmetric pair of side illuminations with an automatic data acquisition program detected the protrusions is developed in this study. The teaching results show smaller compensation in front of the illumination, irrespective of thin-film types. There is larger compensation at the central region for the BM film sample. On the other hand, colored film samples show smaller offsets at the center due to their higher

reflectivity. The result is a 6% error for the BM ball to indicate the greatest difference among PRs. In addition, it also is the farthest away from the 3σ deviation at 23 μm in contrast to the protrusions of red, green, and blue at 15 μm, 18 μm, and 20 μm, respectively. The method can detect the protrusive defects to prevent damage for the photomask with an accurate rate to 94%, irrespective of the thin-film types. The results conform to the criterion within 90% in the TFT-LCD industry.

References

1. Tzu F. M., Chou J. H. Protrusive detection for thin film transistor-liquid crystal display using side-view illumination. IEEE, International Microsystems, Packaging, Assembly and Circuits Technology Conference (IMPACT) **2016**, 416-419
2. Kamali B., Asiaei S., Beigzadeh B., Ebadi A. A. Micro-lithography on paper, surface process modifications for biomedical performance enhancement. Colloids and Surfaces a-Physicochemical and Engineering Aspects **2018**, 555, 389-396
3. Kwon M., Ju Y. G. Microscope projection photolithography based on ultraviolet light-emitting diodes. European Journal of Physics **2018**, 39
4. Hamamoto K., Tanaka Y., Lee S. Y., Hosokawa N., Sakaya N., Hosoya M., et al. Mask defect inspection using an extreme ultraviolet microscope. Journal of Vacuum Science & Technology B **2005**, 23, 2852-2855
5. Park M., Yi M., Mirkarimi P., Larson C., Bokor J. Characterization of extreme ultraviolet lithography mask defects by actinic inspection with broadband extreme ultraviolet illumination. Journal of Vacuum Science & Technology B **2002**, 20, 3000-3005
6. Ishii A. 3-D Shape Measurement Using a Focused-Section Method. Pattern Recognition, 2000 Proceedings 15th International Conference on IEEE **2000**, 4, 828-832
7. Ahmad M. B., Choi T. S. Application of three dimensional shape from image focus in LCD/TFT displays manufacturing. IEEE Trans Consum Electron **2007**, 53, 1-4
8. Zhang R., Tsai P. S., Cryer J. E., Shah M. Shape from shading: A survey. IEEE Trans Pattern Anal Mach Intell **1999**, 21, 690-706
9. Antonacci G. Dark-field Brillouin microscopy. Optics Letters **2017**, 42, 1432-1435
10. Zhang Y. H., Yang Y. Y., Li C., Wu F., Chai H. T., Yan K., et al. Defects evaluation system for spherical optical surfaces based on microscopic scattering dark-field imaging method. Applied Optics **2016**, 55, 6162-6171

11. Nayar S. K., Ikeuchi K., Kannde T. Surface reflection: physical and geometrical perspectives. IEEE Trans Pattern Anal Mach Intell **1991**, 17, 611-634